Journal of Inflammation Research Dovepress

Open Access Full Text Article ORIGINAL RESEARCH

Comparison of the Cecum Ligation and Puncture Method and the Intraperitoneal Lipopolysaccharide Injection Method for the Construction of a New-Onset Atrial Fibrillation Model of Sepsis

Xiuwen Ling[1,*], Jun Shen[2,*], Junqing Liang[2], Kai Yang[1], Jianzhong Yang[1]

[1]Emergency & Trauma Center, The First Affiliated Hospital of Xinjiang Medical University, Xinjiang, People's Republic of China; [2]Cardiac Pacing and Electrophysiology Department, The First Affiliated Hospital of Xinjiang Medical University, Urumqi, Xinjiang, People's Republic of China

*These authors contributed equally to this work

Correspondence: Jianzhong Yang, Emergency & Trauma Center, The First Affiliated Hospital of Xinjiang Medical University, Urumqi, Xinjiang, 830011, People's Republic of China, Tel/Fax +86 18040399020, Email 18040399020@163.com

Background: New-onset atrial fibrillation (AF) in sepsis significantly impacted patient morbidity and mortality, yet the optimal animal model for studying this condition remains undetermined. This study aimed to establish a stable animal model for new-onset AF in sepsis and to explore the molecular mechanisms involved.

Methods: Forty-seven Sprague-Dawley rats were utilized, with the cecal ligation and puncture (CLP) group divided into 0.6 mm and 1.0 mm needle outer diameter subgroups, and the lipopolysaccharide (LPS) group into 5 mg/kg, 10 mg/kg, 15 mg/kg, and 20 mg/kg dosage subgroups. The incidence of new-onset AF and five-day mortality rates were compared to identify the most stable modeling conditions. Selected subgroups underwent further analysis, including cardiac ultrasound, electrophysiology, and pathological examinations. Inflammation-related molecular levels in the atrium were assessed using ELISA and Western blotting (WB).

Results: The intraperitoneal injection of 10 mg/kg LPS was identified as the most stable model for new-onset AF in sepsis, with significant findings including increased left atrial area and fibrosis, left ventricular pump dysfunction, uncoordinated ventricular wall motion, and impaired electrical impulse conduction. The effective atrial refractory period was markedly shorter, and susceptibility to AF was higher in the LPS group compared to the CLP group. Molecular analysis revealed elevated levels of NOD-like receptor protein 3(NLRP3) inflammasomes, apoptosis-associated speck-like protein containing a CARD(ASC), Caspase-1 p20 Elevated levels of three inflammation-related proteins and increased activity of the Sphingosine 1-phosphate/Sphingosine 1-phosphate Receptor 2(S1P/S1P2) signaling axis.

Conclusion: Intraperitoneal injection of 10 mg/kg of LPS can successfully construct a new-onset AF model in sepsis, and NLRP3 inflammatory vesicles mediated by the S1P/S1P2 signaling axis may promote new-onset AF in sepsis.

Keywords: sepsis, atrial fibrillation, rat model, lipopolysaccharide, NLRP3 inflammasome, S1P/S1P2 signaling axis

Introduction

Sepsis was a critical systemic inflammatory response syndrome triggered by infection.[1,2] It was frequently associated with cardiac arrhythmias, particularly AF, which was the most prevalent arrhythmia in this context.[3] AF that arises during sepsis and was not present beforehand is termed new-onset AF in sepsis.[4]

Patients who develop new-onset AF during sepsis exhibited a significantly elevated five-year risk of hospitalization for heart failure compared to those without AF.[5] Moreover, survivors of sepsis with new-onset AF were prone to recurrent AF post-discharge and face increased long-term risks of in-hospital mortality, post-discharge mortality, heart failure, ischemic stroke, and overall mortality.[6,7] The pathophysiological mechanisms underlying new-onset AF in

Received: 20 August 2024
Accepted: 26 October 2024
Published: 19 November 2024

sepsis were not well understood and may be distinct from those of AF in non-septic contexts. The development of stable animal models for sepsis-induced new-onset AF was challenging. Current approaches involved creating models through genetic engineering to induce spontaneous AF or by electrically stimulating the left atrium to provoke AF, with large animals such as horses, pigs, and dogs being the typical subjects.[8–10] However, the complexity and expense of these methods hindered high-throughput experimental research into the pathogenesis and treatment of sepsis-induced AF.

The primary sepsis models currently in use include CLP and intraperitoneal injection of LPS.[5] The severity of sepsis in CLP models has been categorized, with approximately two-thirds cecum ligation representing a model for severe sepsis,[11] which means that this modeling modality has the highest level of inflammation and may be better suited to explore the relationship between inflammation and new-onset atrial fibrillation. Both CLP and LPS models in mice and rats have demonstrated the occurrence of arrhythmias in sepsis, including AF.[12,13] However, the optimal model for studying new-onset AF in sepsis remained to be determined.

Materials and Methods

Animal Preparation and Study Protocol

Forty-seven Sprague-Dawley rats were acquired from the Animal Experiment Center at Xinjiang Medical University, and all procedures involving animals were conducted at the Xinjiang Key Laboratory of Cardiac Electrophysiology and Electroreconstruction, affiliated with the First Hospital of Xinjiang Medical University. Ambulatory electrocardiograms were obtained using a TER010 patch-type electrocardiograph one day prior to the experimental modeling. The rats were randomly assigned to four groups: control(CT) (n=6), sham operation (n=6), CLP(n=24), and LPS treatment (n=11). The CLP group was subjected to a 12-hour fast followed by cecum ligation, puncture, and fecal extrusion to induce infection. The LPS group received intraperitoneal injections of LPS (L2880, sigma, German) (5 mg/kg, 10mg/kg, 15 mg/kg, and 20 mg/kg) post-fasting. On the fourth day post-modeling, we performed tracheal intubation and chest opening in rats under anesthesia, atrial electrophysiology studies were performed on all rats. The optimal recording was identified by the LEAD-7000 Multi-Conductive Physiological Recorder (Figure 1A).

Measurement of Effective Atrial Refractory Period

The effective atrial refractory period (AERP) was determined by programmed electrical stimulation of the left and right atria separately using the LEAD-7000 Multi-Conductive Physiological Recorder.An 8:1 S1S2 stimulation protocol was employed, utilizing an output voltage of 4 V and a pulse width of 0.5 ms. This consisted of eight consecutive stimuli (S1-S1 interval of 260 ms) followed by a single premature stimulus (S2). The S1S2 interval commenced at 110 ms and was progressively reduced in 5-ms decrements until the AERP was identified. The AERP was defined as the longest S1S2 interval that failed to provoke a response. Each rat underwent three trials, and the mean of these trials was recorded as the AERP for the respective atrium. The procedure was replicated three times per rat, and the average of these measurements was considered the definitive AERP for the experimental subject.

Measurement of AF Induction Rate

The induction rate of AF was assessed using the burst stimulation method. This involved applying an S1S1 protocol with an 8 V voltage and a frequency of 50 hz for 10 seconds per stimulation. Following each stimulation, the presence of AF was determined, and typical screenshots were captured for documentation. Subsequent stimulations were administered at 5-minute intervals, with a total of three stimulations per rat. Persistent AF, defined as lasting 1000 ms or longer, was terminated using S1S1 stimulation, and the subsequent burst stimulation was initiated after a 5-minute recovery period. The AF induction rate was calculated as the percentage of successful AF inductions. In this study, AF was characterized by the absence of the p-wave, replaced by irregular f-waves, and a duration exceeding 1000 ms.

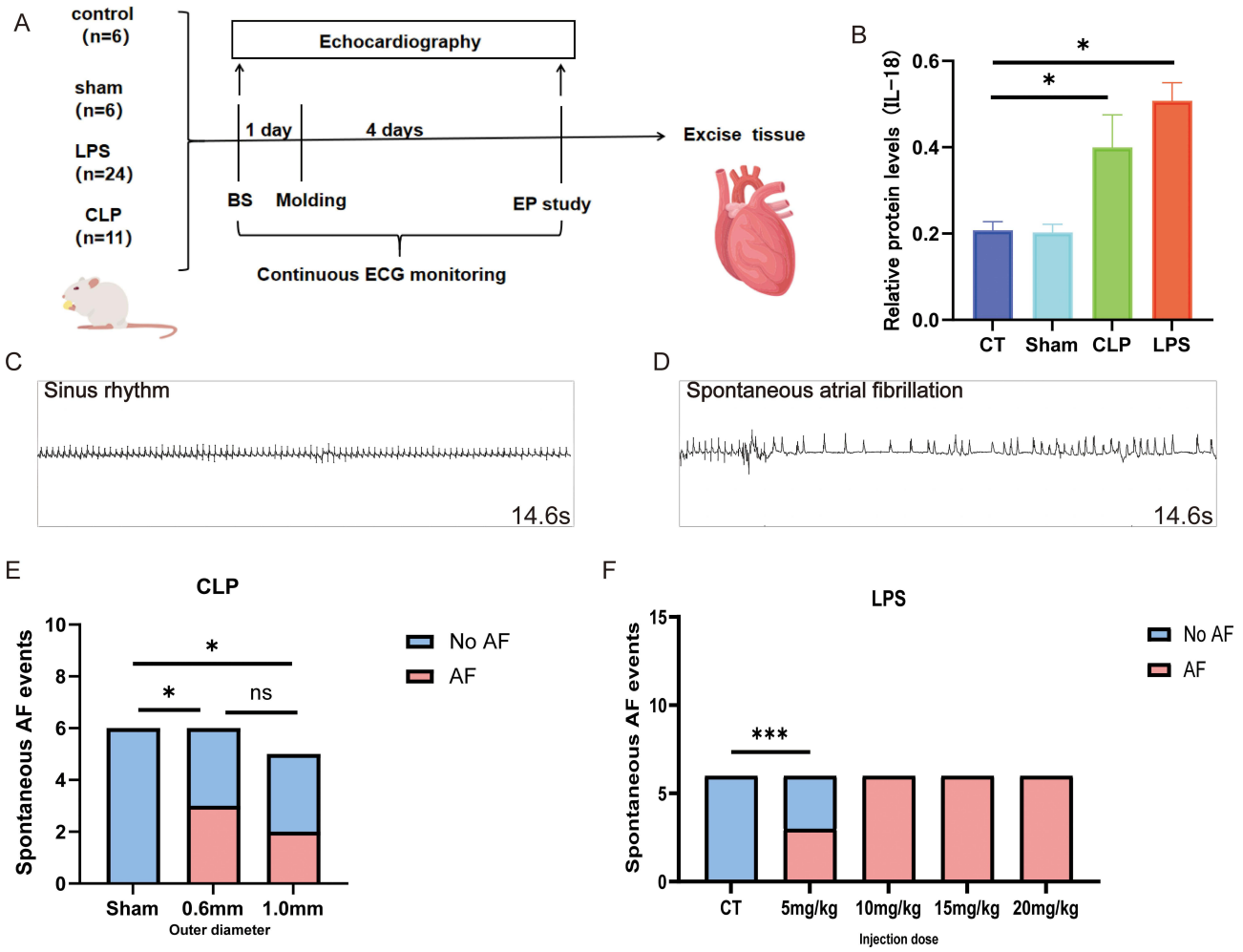

Figure 1 Schematic diagram of molding process.(**A**)Flowchart of molding and related metrics measurement; (**B**) The relative protein levels of IL-18 were determined by centrifugation of blood in each group and the supernatants were collected for the elisa assay four days after the completion of modeling. (**C** and **D**) Sinus rhythm and AF observed by analyzing surface electrocardiogram data; (**E**) Statistics of new-onset AF occurrences in each subgroup of the CT group and the LPS group; (**F**) Statistics of new-onset AF occurrences in the Sham group and the CLP subgroup; *p<0.05, ***p<0.001, labeled as ns when p>0.05. Data are expressed as mean ± SEM. n=6/group, n=5 (1.0 mm group).

Abbreviations: BS, baseline; EP, electrophysiology.

Measurement of Left Atrial Electrical Conduction Velocity and Heterogeneity

In vivo microelectrode array (MEA) recordings were employed to evaluate the conduction velocity and heterogeneity within the left atrium of rats. The rats were anesthetized, mechanically ventilated, and positioned on the operating table at the MEA facility. A median sternotomy was performed using bone scissors, and the ribs were gently spread with a rib spreader to fully reveal the heart. A flexible MEA was placed on the left atrial surface. Following the stabilization of unipolar electrical signals from the MEA, conduction maps were produced during sinus rhythm. The data were collected at a sampling rate of 10 kHz per channel and processed using Cardio2D+ software. Left atrial electrograms were acquired and a set of left atrial conduction velocities were measured from five consecutive stable heartbeats, and the mean of the conduction velocities (CV) was calculated after excluding outliers. The variance of each set of conduction velocity data was calculated after excluding outliers, and was used as heterogeneity of conduction velocities to quantify conduction heterogeneity to mitigate the effects of conduction instability.

Echocardiography

All animals were anesthetized with isoflurane, appropriate room temperature and animal heating pads using a Doppler ultrasound machine for measurements of cardiac ultrasound related data. All animals were traced in left ventricular(LV) long-

axis views while awake using a Doppler ultrasound machine, (Philips Corporation, Bothell, WA, USA) using a S12-4 scanning probe. The following specific parameters were measured for at least three consecutive heartbeats: Left atrial diameter, Left ventricular ejection fraction (LVEF) and early mitral peak velocity to atrial peak velocity ratio(E/A) peaks.

Histological Analysis

Left atrial tissues were fixed in 4% paraformaldehyde for 24 hours and subsequently embedded in paraffin. Hematoxylin and eosin (H&E) staining, as well as Masson's trichrome staining, were conducted on tissue sections measuring 3 μm in thickness. Inflammatory infiltrates usually result in inflammatory cells congregating around the damaged tissue, and areas of inflammatory cell infiltration with a high density of inflammatory cells are visible on microscopic observation of HE-stained pathology sections. While the areas staining positive for collagen in the Masson's trichrome sections denoted the extent of cardiac fibrosis. Quantification of inflammatory cell infiltration and fibrosis was performed using a single bright-field microscopy image from each animal at 200× magnification. Image analysis was carried out using ImageJ software (version 1.8.0).

ELISA Assay

Plasma samples from SD rats were analyzed for Interleukin-18 (IL-18) concentration using an ELISA kit (CSB-E04610r, Cusabio, China). A volume of 100 μL of the appropriately diluted samples was added to the pre-coated wells, alongside blank and standard wells containing serial dilutions. The plate was sealed with a cover film and incubated at 37°C for 1–2 hours. Following incubation, wells were washed and then incubated with 100 μL of biotinylated antibody working solution at 37°C for 1 hour. After a subsequent wash, 100 μL of enzyme conjugate working solution was added to each well. Post-washing, TMB substrate solution was dispensed into each well and the reaction was allowed to proceed at 37°C for 10–30 minutes until a color gradient was observed in the standard wells. The reaction was stopped by adding 100 μL of 2M sulfuric acid to each well, resulting in a color change from blue to yellow. Within 10 minutes, the optical density (OD) at 450 nm was measured using a microplate reader, with zero adjustment based on the blank control well. A standard curve was generated from the OD values of the standards, and sample concentrations were calculated using the curve equation. Results were recorded in an Excel spreadsheet.

Western Blotting

Left atrial homogenates were prepared using a mixed cell lysate solution (RIPA: PMSF: Phosphatase Inhibitor Cocktail = 100:1:1, Solarbio, China). The protein concentration was quantified with a BCA assay kit (PC0020, Solarbio, China). Subsequently, 20 μg of protein per sample was subjected to electrophoresis on a 10% SDS-PAGE gel at 80 V for 140 minutes using a Mini-PROTEAN system (Bio-Rad). The separated proteins were then transferred onto PVDF membranes via wet transfer at 300 mA for 90 minutes. Membranes were blocked with 5% BSA for 1 hour at room temperature and incubated with primary antibodies overnight at 4°C. Experiments using X-Ray film darkroom exposures. The primary antibodies utilized included anti-ASC (AB307560, Abcam, USA), anti-NLRP3 (SAB5700723, Sigma, USA), anti-Caspase-1 (89332, Cell Signaling Technology, USA), anti-S1P (AB140592, Abcam, USA), anti-S1P2 (AB235919, Abcam, USA), and GAPDH (10494-1-AP, Proteintech, USA).

Statistical Analysis

The raw data were entered into Excel (version 2024, WPS) and analyzed using SPSS (version 25.0) to compare differences in rates between groups. GraphPad Prism (version 9.0) was employed for the analysis and visualization of continuous variables. Data were presented as mean ± Standard Error of Mean. The event rates across the four groups were assessed using Fisher's exact test, as the conditions for the chi-square test were not met due to the requirement that each cell should contain more than one event. For the comparison of continuous variables across multiple groups, one-way ANOVA was conducted. A p-value of less than 0.05 was considered indicative of statistical significance.

Results

The Most Stable Model of New-Onset AF in Sepsis Constructed by Intraperitoneal Injection of 10 Mg/Kg LPS

Compared with the CT group, rats in the CLP and LPS groups were significantly depressed, fed less, were less active, had less self-cleaning behavior, had significantly messy fur, and were curled up; there was no obvious avoidance of the grasping response; the stools were pasty, and there was an increase in the periocular secretion. Inflammatory factor levels were significantly higher in the rats of the CLP and LPS groups than in those of the CT and Sham groups (Figure 1B). New-onset atrial fibrillation in sepsis was found in both CLP and LPS groups (Figure 1C and D), and the incidence of new-onset AF in sepsis did not differ significantly among subgroups of CLP with different outer diameters (ODs) (Figure 1E), and among subgroups of LPS, the low mortality rate and the high incidence of new-onset AF in the 10 mg/kg group was statistically significantly different from that in the other groups (Figure 1F and Supplementary Figure 1).

Echocardiography Findings of AF in the LPS Group

Echocardiography via the LV long-axis view revealed a significant enlargement of the left atrium in both the CLP and LPS groups when compared to the CT and Sham groups (Figure 2E). The analysis of left atrial diameter changes pre-modeling and post-modeling indicated that the CLP and LPS groups experienced marked left atrial dilation, whereas the CT and Sham groups exhibited minimal alterations in left atrial size (Figure 2B). Additionally, the CLP and LPS groups demonstrated notable incoordination in ventricular wall motion (Figure 2A). And the studies documented the absence of peak A and the emergence of a singular peak in the mitral M-curve and mitral valve flow profile in the experimental groups as opposed to the CT group (Figure 2F). Specifically, in the LPS group, the E/A peak velocity ratio was significantly reduced relative to the CT group (Figure 2D), and a more pronounced decrease in LVEF was observed, indicating a substantial impairment in LV pump function (Figure 2C).

Reduced Effective Atrial Refractory Period and Enhanced AF Susceptibility in the CLP and LPS Groups

In the CT and sham groups, the effective refractory periods (ERP) of the left and right atria ranged between 70–80 ms. In contrast, the CLP and LPS groups exhibited significantly reduced ERPs, oscillating between 15–20 ms, with statistically significant differences observed (Figure 3E and F). Typical images of AF induction with burst pacing at 40 ms S1-S1 interval among four groups. (Figure 3A–D). Furthermore, the rate of AF induction in the CLP group was markedly higher than in the Sham group (Figure 3G). Similarly, the LPS group demonstrated a significantly elevated AF induction rate compared to both the Sham group (Figure 3G) and the CT group (Figure 3G). Notably, the AF induction rate in the LPS group also surpassed that of the CLP group (Figure 3G).

Impaired Electrical Impulse Conduction in the LPS and CLP Groups

The CT and Sham group images exhibit consistent electrical impulse conduction directions, as indicated by the arrows, along with orderly equipotential line distribution and uniform conduction patterns. Conversely, the CLP and LPS group images reveal disordered conduction directions, irregular equipotential line distribution, and apparent impediments to electrical impulse propagation (Figure 4A). The conduction velocity in the lipopolysaccharide (LPS) group was significantly reduced compared to the CT group (Figure 4B). Similarly, the cecum ligation and puncture (CLP) group exhibited a markedly decreased conduction velocity relative to the sham-operated (Sham) group (Figure 4B). However, no significant difference in conduction velocity was observed between the CLP and LPS groups (Figure 4C).

Enhanced Inflammatory Response and Atrial Fibrosis in the LPS Group Relative to the CLP Group

Hematoxylin and eosin (H&E) staining revealed an absence of inflammatory cell infiltration in the CT and Sham groups, while significant infiltration was observed in both the CLP and LPS groups. Quantitative analysis showed a statistically significant

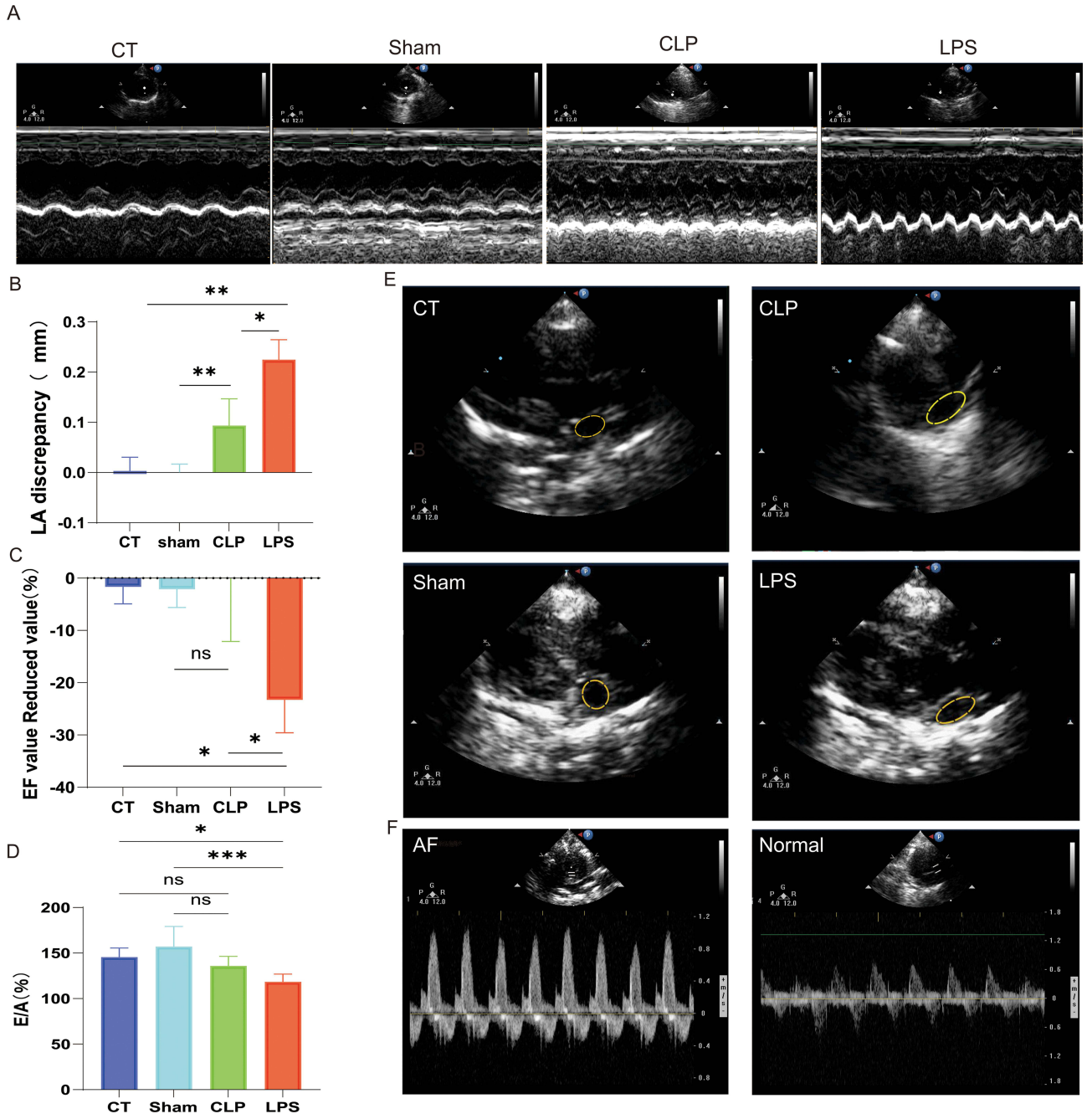

Figure 2 Impact of LPS on Cardiac Morphology and Function. (**A**) Coordination of ventricular wall motion in rats of each group; (**B**) Enlarged area of the left atrium; (**C**) Reduced values of EF values; (**D**) E/A peak percentage; (**E**) in order, represent the area of the left atrium of CT, Sham, CLP, and LPS groups observed in long-axis views of the left ventricle; (**F**) Single-peak image of the E/A peak of AF observed with M-mode ultrasound and normal image of the E/A peak; *p<0.05,**p<0.01,***p<0.001, labeled as ns when p>0.05. Data are expressed as mean ± SEM. n=6/group.

greater extent of inflammatory cell infiltration in the LPS group compared to the CLP group (Figure 5A and B). Masson's trichrome staining indicated pronounced atrial myofibrosis in the CLP and LPS groups relative to the CT and Sham groups, with the degree of fibrosis being significantly higher in the LPS group (Figure 5A and C). Immunohistochemical analysis demonstrated that the LPS group exhibited the most abundant NLRP3 inflammasomes within the cytoplasm of atrial myocytes, as indicated by the stained area in the NLRP3 immunohistochemistry images (Figure 5A and D). Furthermore, a positive correlation was identified between the presence of NLRP3 inflammasomes, myocardial fibrosis, inflammatory cell infiltration, and the incidence of new-onset AF in sepsis. During an inflammatory response, an increase in NLRP3

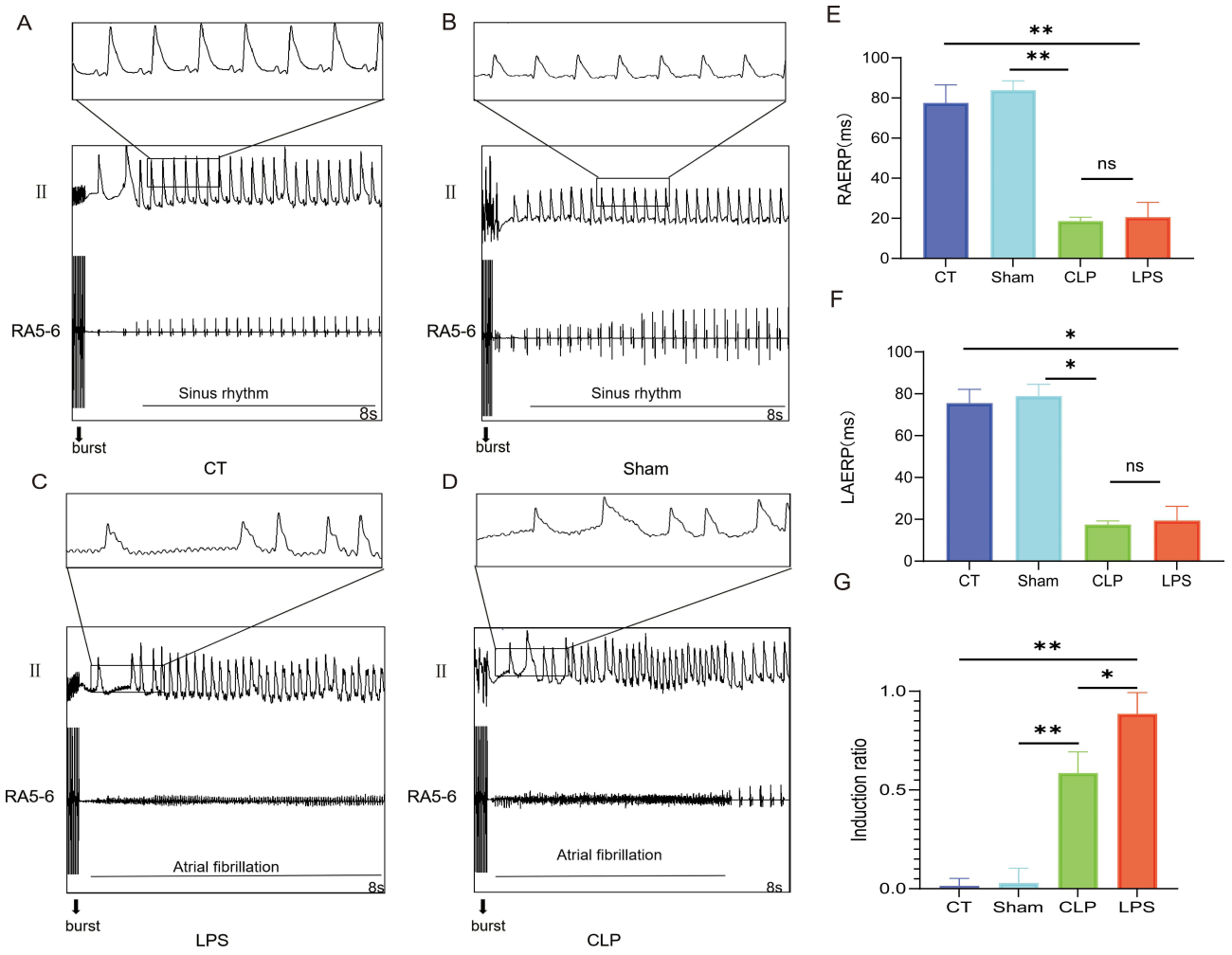

Figure 3 Impact of LPS on ERP in right and left Atria and the Incidence of AF Induction. (**A**–**D**) the electrocardiographic performance of rats after electrical stimulation; (**E** and **F**) the effective atrial refractory period of the left and right atria; (**G**) the rate of AF induced in each group of rats; *p<0.05,**p<0.01, labeled as ns when p>0.05. Data are expressed as mean ± SEM. n=6/group.

inflammasomes in cardiomyocytes is observed, along with a concomitant rise in caspase-1, a component of the NLRP3 inflammasomes.[14] This elevation promotes the activation of IL-1β precursors, leading to increased levels of these cytokines and associated myocardial fibrosis (Figure 5A and E).

Elevated NLRP3 Inflammasome and S1P/S1P2 Signaling in the LPS Group Relative to the CLP Group

The pathogenesis of new-onset AF in sepsis has remained elusive. Western blot (WB) assays targeting the NLRP3 inflammasome and the upstream S1P/S1PR2 signaling axis revealed significant upregulation of NLRP3, ASC, and the active form of caspase-1 (caspase1-p20) in both CLP and LPS groups, with a more marked increase in the LPS group (Figure 6A–E). These findings imply a potential positive correlation between NLRP3 inflammasome activity and the risk of new-onset AF in sepsis. Furthermore, reduced sphingosine-1-phosphate concentrations in the CLP and LPS groups signified augmented inflammation. Concomitantly, heightened expression of its receptor, S1P2, implies that the potentiation of the inflammatory response through the S1P/S1P2 signaling pathway might escalate the risk of sepsis-induced AF (Figure 6F and G).

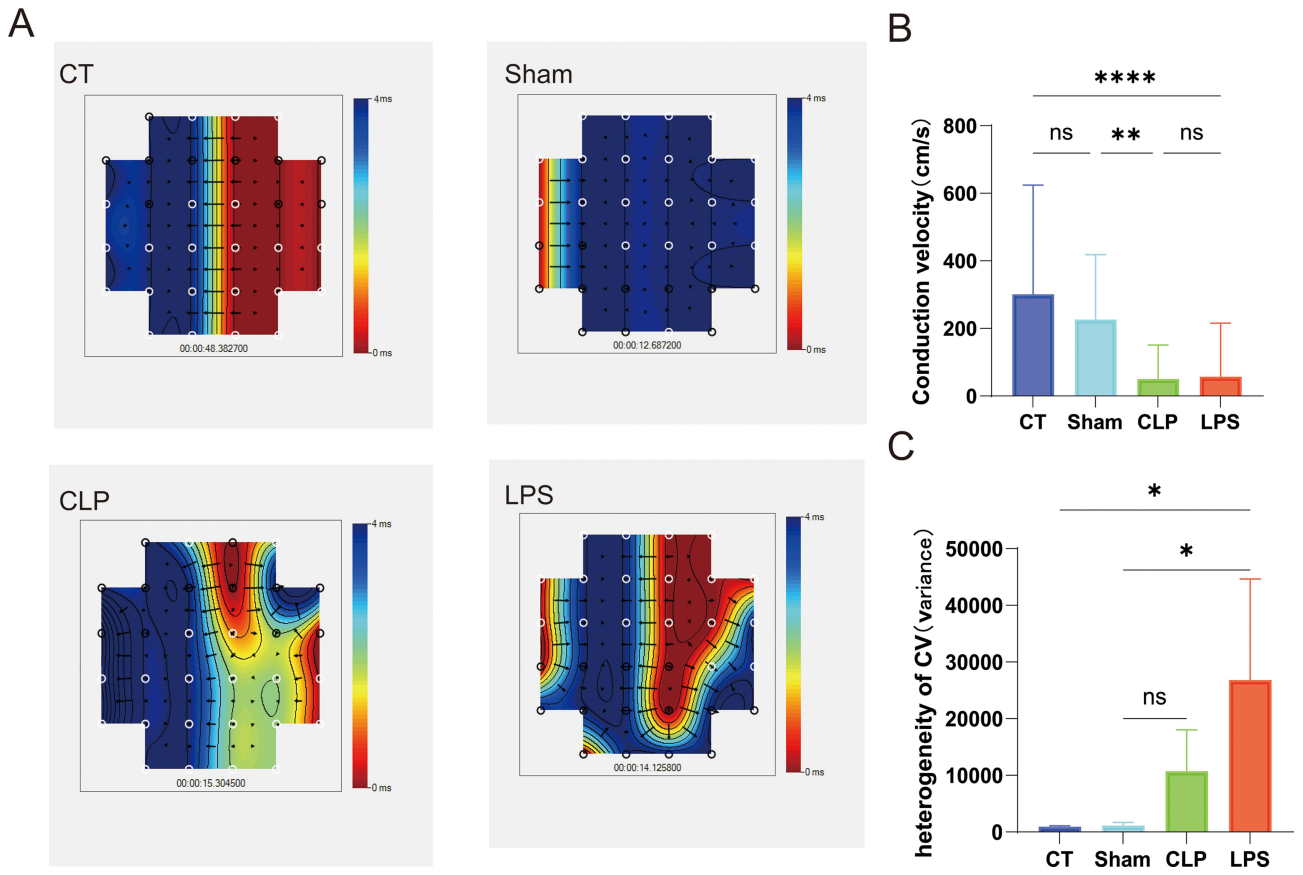

Figure 4 Influence of LPS on Conduction Velocity and Its Variability in Cardiac Tissue. (**A**) Microarray electrode thermograms of electrical conduction in rats from each group, arrows represent the direction of conduction, different colors represent the moment of impulse arrival, and contour lines represent the location of electrical impulse conduction at the same moment; (**B**) the left atrial conduction velocity measured in each group; (**C**) the heterogeneity of the left atrial conduction velocities of the groups (as reflected by calculating the variance). *p<0.05,**p<0.01,****p<0.0001, labeled as ns when p>0.05. Data are expressed as mean ± SEM. n=6/group.

Discussions

The CLP model is widely regarded as one of the most representative animal models of human sepsis due to its ability to induce multiple organ dysfunction syndrome (MODS) and replicate clinical sepsis by facilitating the entry of intestinal bacteria and toxins into the peritoneal cavity via mechanical perforation,[15–17] eliciting a comprehensive immune response. Nevertheless, the CLP procedure is complex, necessitates a high level of technical expertise, demands rigorous postoperative care, and yields results with limited reproducibility.[18,19] In contrast, the LPS model is straightforward to implement, offers high reproducibility, allows for the modulation of the inflammatory response through dosage adjustments, and results in severe pathological changes.[20] It is therefore more suitable for modeling endotoxin-induced acute inflammatory responses and for observing and evaluating the efficacy of anti-inflammatory drugs.[21]

Research on new-onset AF in sepsis and the predisposition to AF during sepsis is limited. Our study demonstrated that sepsis models induced by intraperitoneal injection of 10 mg/kg LPS exhibited a heightened incidence of new-onset AF and an increased vulnerability to AF. Despite the advantages and disadvantages associated with both CLP and intraperitoneal LPS methods, our findings indicated that the LPS-induced sepsis model had a higher frequency of spontaneous AF and greater susceptibility to the condition. The consistency of these results across multiple independent experiments was notable, with the occurrence of new-onset AF, inflammatory responses, electrophysiological abnormalities, significant reductions in the effective refractory periods of left and right atrial fibers, and pronounced atrial fibrosis. Statistical analysis confirmed the significance of these differences. Literature review suggests that intraperitoneal injection LPS is more likely to cause spontaneous and inducible AF events.[22] This may be attributed to the LPS-induced inflammatory response, which promotes inflammation and structural remodeling of cardiac tissues, including atrial

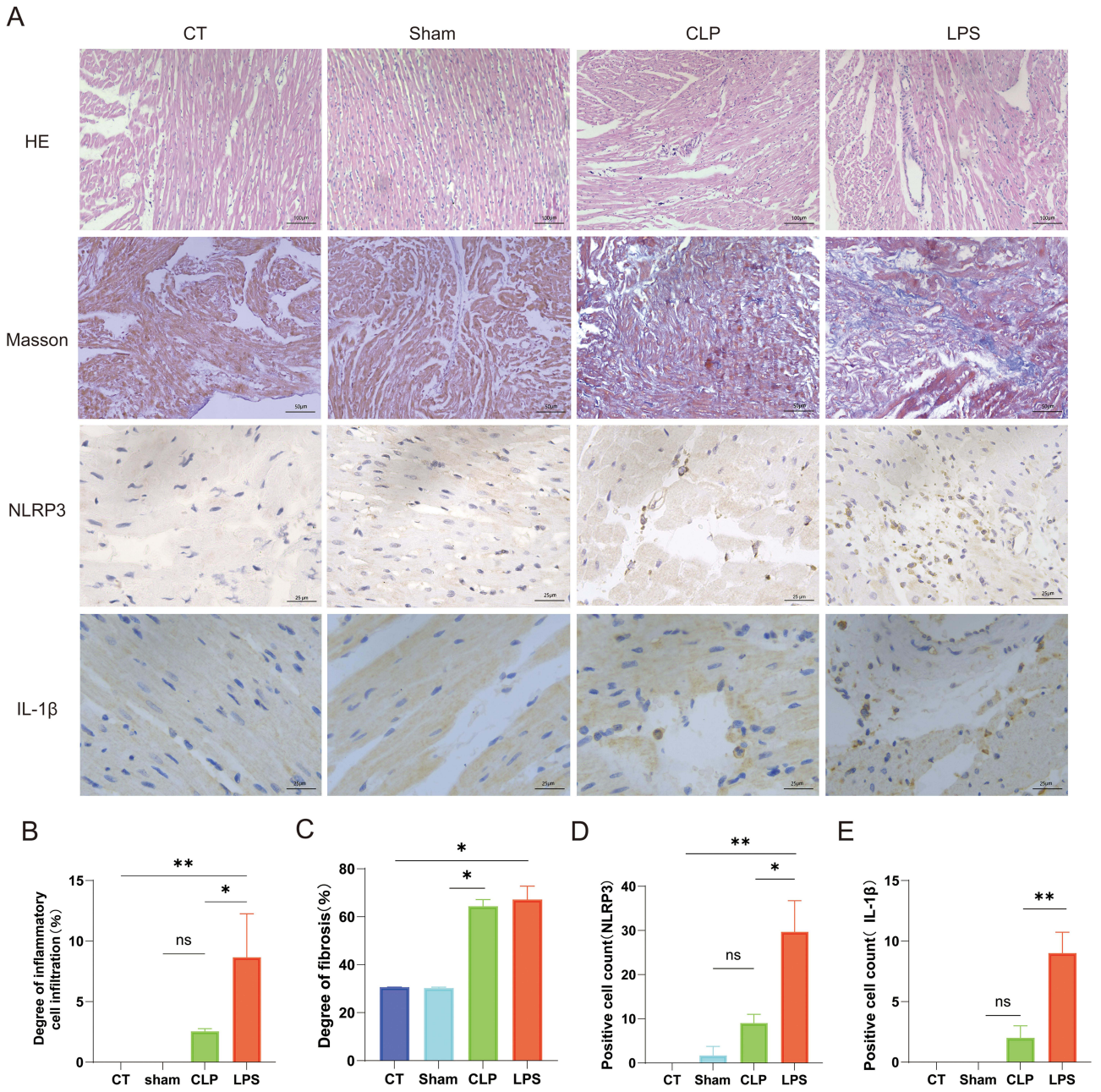

Figure 5 Impact of LPS on Pathological Alterations in Atrial Myocytes. (**A**) The HE staining results, Masson's trichrome staining, NLRP3 inflammatory vesicles immunohistochemistry results, and IL-1β immunohistochemistry results of rat atria in each group observed under the microscope. (**B**) the statistical graph of the degree of inflammatory cell infiltration; (**C**) the statistical graph of the degree of atrial myofibrillar fibrosis, (**D**) the statistical graph of the counts of positive cells with cytoplasmic containing NLRP3 inflammatory vesicles, (**E**) the statistical graph of the counts of positive cells with cytoplasmic containing IL-1β,*p<0.05,**p<0.01, labeled as ns when p>0.05. Data are expressed as mean ± SEM. n=3/group.
Abbreviation: IL-1β, Interleukin-1 beta.

fibrosis and cardiomyocyte apoptosis.[23,24] Such alterations enhance the electrical heterogeneity of the atria, predisposing them to abnormal electrical activity and subsequent AF. Inflammatory mediators may also directly influence cardiac electrophysiological properties, increasing AF risk by affecting ion channel function, extending action potential duration, and shortening the effective refractory period.[25] This model facilitates the investigation of inflammatory mediators in cardiac electrophysiological abnormalities, elucidates the specific mechanisms by which sepsis induces cardiac complications, and enables the assessment of new drugs and therapeutic strategies for sepsis-induced AF. Moreover, the model

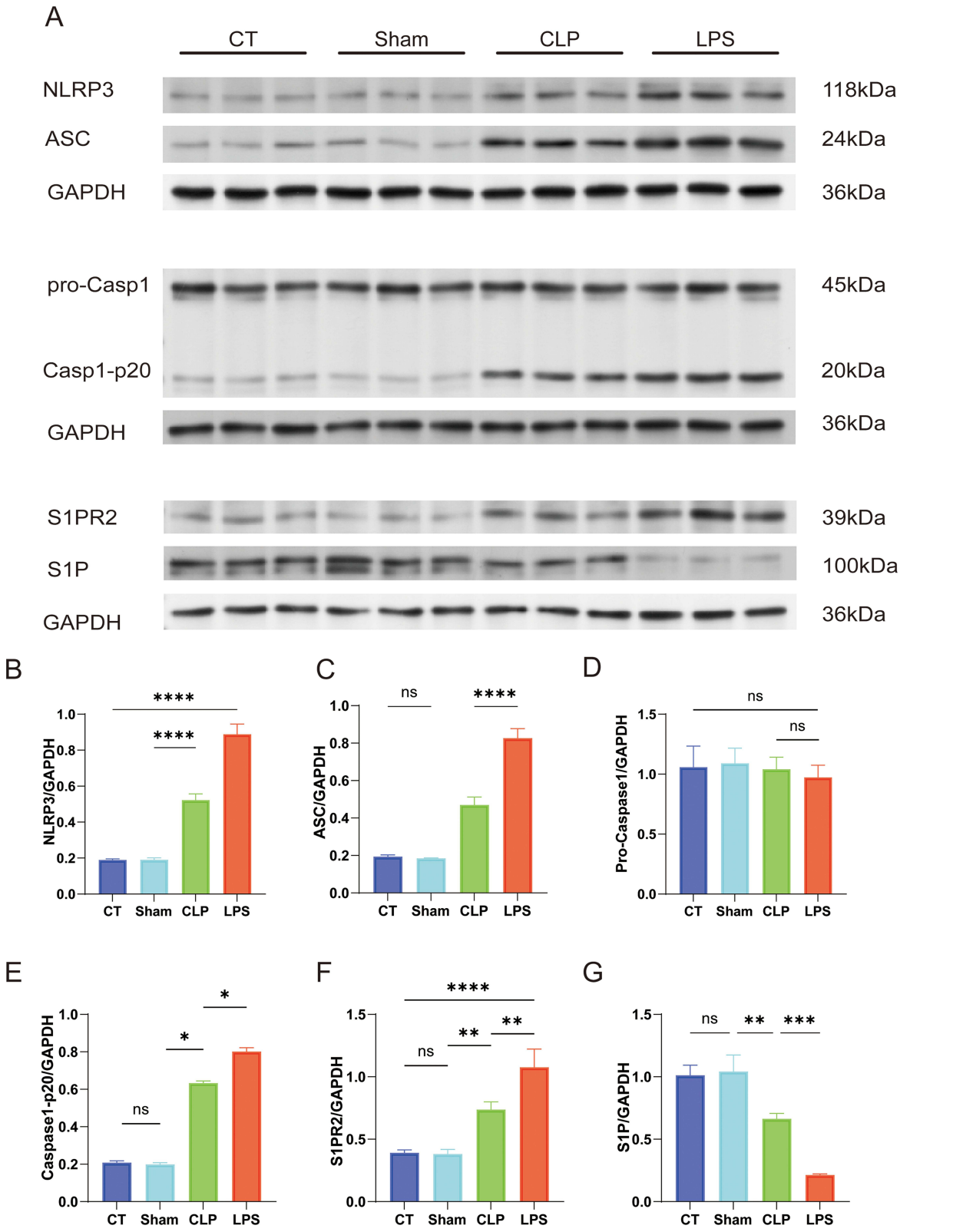

Figure 6 Quantitative Analysis of Inflammatory and Signaling Protein Expression Relative to GAPDH in Atrial Myocytes. Differential analysis in protein expression levels between four groups. (**A**) Immunoblotting for the detection of protein bands in developed results (**B**) ratio of NLRP3 protein expression level to GAPDH protein expression level; (**C**) ratio of ASC protein expression level to GAPDH protein expression level; (**D**) ratio of Pro-Caspase1 protein expression level to GAPDH protein expression level; (**E**) ratio of Caspase1-p20 protein expression level to GAPDH protein expression level; (**F**) ratio of S1P2 protein expression level to GAPDH protein expression level; (**G**) ratio of S1P protein expression level to GAPDH protein expression level;*p<0.05,**p<0.01, ***p<0.001, ****p<0.0001, labeled as ns when p>0.05. Data are expressed as mean ± SEM. n=3/group.

may assist in identifying biomarkers for sepsis-related cardiac injury and new-onset AF, offering potential benefits for diagnosis and personalized treatment approaches.

Electrocardiography is the method of choice for diagnosing AF, revealing both electrocardiographic alterations and associated changes in cardiac structure and hemodynamics, which are detectable via echocardiography.[26] Left atrial diameter serves as a critical metric for evaluating left atrial structure. Enlargement of the left atrium contributes to extended electrical conduction pathways and augmented electrical heterogeneity, thereby facilitating re-entry loop formation and predisposing to AF.[27] Experimental models have demonstrated that left atrial enlargement is more pronounced in the LPS group than in the CLP group. During AF, peak A of the mitral inflow spectrum are absent,[28] resulting in a singular peak Although the E/A peak ratio in the CLP and LPS groups exhibited alterations, it did not reach the diagnostic threshold for abnormality (E/A peak ratio < 1). The E/A ratio measured in this study, may be attributed to LV stiffness and elevated left atrial pressure, resulting in a "pseudo-normal" filling pattern. Rats with atrial fibrillation may develop myocardial fibrosis, leading to structural remodelling of the heart, which results in left ventricular stiffness and left atrial pressure. The meaning of E/ A is an index for assessing ventricular diastolic function.[29,30] Where E represents the filling peak of the left ventricle that fills rapidly during early diastole and the A peak is the filling peak of the left ventricle that fills during late diastole, so that under normal conditions E/A>1. Normally, blood flow through the AV valve into the left ventricle should be predominantly in early diastole. AF is characterized by atrial pump failure, rapid and irregular ventricular rates, leading to ventricular underfilling and systolic dysfunction.[31] This dysfunction manifests as ventricular wall motion discrepancies on echocardiography,[31] which were notably evident in the LPS group. LVEF is a primary indicator of LV systolic function. In sepsis, a decline in LVEF may result from systemic inflammation and myocardial depression, indirectly heightening the risk of elevated LV pressures and AF development. The significant impairment in LV pump function among subjects with sepsis can be explained by several sepsis-induced mechanisms, including systemic inflammation, oxidative stress, mitochondrial dysfunction, calcium handling abnormalities, and the release of cardiodepressant factors, all of which can contribute to cardiac dysfunction. sepsis as a comprehensive cardiac impairing agent, which may incite AF by ventricular diastolic dysfunction.[32,33] Echocardiography enables the early detection of cardiac structural and functional changes, facilitating the prompt identification of septic patients at elevated risk for AF.[34] Early diagnosis allows for timely interventions to mitigate the incidence of AF and its associated complications.

Shortening of the effective refractory period (ERP) reduces the repolarization duration in atrial myocardium, enhances repolarization disparity, and fosters the emergence of multiple repolarization wavefronts.[35] This disparity amplifies electrical heterogeneity among atrial muscle fibers, facilitating localized ectopic excitation that can initiate and perpetuate AF.[36] A shortened ERP permits quicker restoration of excitability in the atrial myocardium, heightening the probability of reentrant circuits. Such circuits are a key mechanism in AF pathogenesis, where rapid recovery and re-excitation of atrial muscle lead to persistent electrical activity loops, contributing to AF onset and persistence.[37] The systemic inflammatory response induced by sepsis triggers the release of numerous inflammatory mediators (eg, TNF-α, IL-6, IL-1β), which downregulate sodium (I_{Na}^{2+}) and calcium (I_{Ca}^{2+}) channel expression,[38,39] impeding depolarization. Concurrently, the expression of specific potassium channels is upregulated, hastening repolarization.[40] Oxidative stress from sepsis impairs ion channel proteins[41] altering their function and diminishing depolarization.[42] Inflammation and oxidative stress together render the electrophysiological attributes of atrial myocytes heterogeneous, which escalates the propensity for reentrant circuit formation and predisposes to AF.[43] Studies indicate that heightened inflammatory mediator levels correlate with compromised sodium and calcium channel functionality, leading to reduced action potential duration and ERP, thus elevating AF risk.

The NLRP3 inflammasome is a multi-component protein complex that is pivotal in mediating inflammation and immune responses.[44] Sepsis, a severe infectious condition often accompanied by AF, may be influenced by various factors, including the activation of the NLRP3 inflammasome.[45] This activation precipitates the secretion of proinflammatory cytokines such as IL-1β and IL-18, which can inflict cardiomyocyte damage and electrophysiological disturbances, consequently elevating the risk of AF.[46] Moreover, the activation of NLRP3 inflammasomes may indirectly contribute to the pathogenesis of AF by instigating oxidative stress and compromising cardiomyocyte functionality.[47] Thus, the activation of NLRP3 inflammasomes during sepsis is a significant contributing factor to the heightened risk of AF through the promotion of inflammatory mediator release and other pathophysiological processes.[48] Sphingosine 1-phosphate (S1P) is a bioactive lipid that interacts with its receptors, such as S1P1 and S1P2.[49] The S1P/S1P receptor signaling pathway, particularly through S1P2, has been implicated

in the regulation of inflammasome formation and activation.[50] S1P2 receptors may facilitate the assembly of NLRP3 inflammasomes and the subsequent discharge of inflammatory mediators.[49]

The systemic inflammatory response elicited by sepsis can result in heightened oxidative stress and an abundance of reactive oxygen species (ROS).[51] These ROS not only inflict direct damage on cardiomyocytes but also amplify inflammation and cellular injury by activating the NLRP3 inflammasome.[51] Persistent inflammation can induce myocardial fibrosis, a structural alteration that disrupts electrical conduction and predisposes individuals to AF.[52] Inflammatory mediators, such as IL-1β, can perturb calcium homeostasis in cardiomyocytes by interfering with calcium channels and regulatory proteins,[53] leading to abnormal excitability and automaticity that increase the propensity for AF. Therapeutic interventions targeting pro-inflammatory cytokines, like IL-1β inhibitors, may mitigate myocardial inflammation and diminish the risk of AF.[54] Additionally, antioxidant treatments could alleviate sepsis-induced oxidative stress, thus safeguarding cardiomyocytes and lowering the occurrence of AF. A multifaceted treatment approach that integrates anti-inflammatory, antioxidant, and myocardial protective strategies may prove more efficacious in the prevention and management of sepsis-associated AF.

Limitations

The pathogenesis of new-onset AF in sepsis remains elusive. It is established that the NLRP3 inflammasome can facilitate the development of AF, and the S1P/S1P2 signaling pathway is known to exacerbate LPS-induced sepsis, leading to the activation of the NLRP3 inflammasome.[55] However, the potential role of the S1P/S1P2 axis in modulating the NLRP3 inflammasome and its subsequent promotion of AF via mitochondrial ROS release has not been fully elucidated. Future research could involve quantifying mitochondrial ROS, inhibiting the S1P/S1P2 pathway with JTE013,[56] targeting the NLRP3 inflammasome with MCC950,[57] and assessing ion channel activity and current changes in atrial myocyte membranes through optical labeling. These approaches may shed light on the specific mechanisms underlying the onset of AF in sepsis.

The assays employed in this study did not provide the comprehensive analysis required for flow cytometry to precisely determine which specific type of inflammatory cell proliferation is most closely linked to the emergence of new-onset AF in sepsis, which is critical for assessing the efficacy of sepsis modeling. Furthermore, the study did not include the application of NLRP3 inflammasome inhibitors or S1P/S1P2 inflammasome inhibitors to ascertain their association with new-onset AF in sepsis.

Conclusion

In our study, we established that an intraperitoneal injection of LPS at a dosage of 10 mg/kg successfully induced a model of new-onset AF in a septic context, characterized by a high incidence of AF and a low mortality rate. This model exhibited electrophysiological alterations and cardiac structural-functional changes that align with the typical presentation of AF. Furthermore, we observed upregulation of NLRP3 inflammasomes and the S1P/S1P2 signaling pathway in the LPS-treated group.

Abbreviations

AF, atrial fibrillation; LPS, lipopolysaccharide; CLP, cecum ligation and puncture method; CT, control; IL-18, Interleukin-18; ERP, effective refractory period; AERP, effective atrial refractory period; LV, left ventricular; LVEF, Left ventricular ejection fraction; E/A peaks, early mitral peak velocity to atrial peak velocity ratio; CV, conduction velocities; HE, Hematoxylin and Eosin stain; ASC, apoptosis-associated speck-like protein containing a CARD; NLRP3, NOD-like receptor protein 3; ODs, outer diameters; BS, baseline; EP, electrophysiology; ROS, reactive oxygen species; S1P, Sphingosine 1-phosphate; IL-1β, Interleukin-1 beta.

Ethics Approval

All animal experiments were conducted in compliance with National Institutes of Health guidelines and were approved by the Animal Research Ethics Committee of the Affiliated Hospital of Xinjiang University.

Acknowledgments

I would like to express my sincere gratitude to all the laboratory mice that were essential to the completion of my experiments. Their role in this research was invaluable, and I am deeply appreciative of their contribution to science. Additionally, my heartfelt thanks go to the team at the Emergency Trauma Center of Xinjiang Medical University and the Cardiac Pacing Electrophysiology Team for their expert assistance and valuable insights. Their dedication and hard work laid the foundation for the smooth progression of this study. I am also grateful to my supervisor and colleagues for their encouragement and support throughout this journey. Each member's contribution has been an integral part of this article. Thank you once again.

Funding

This work was sponsored by the National Natural Science Foundation of China (grant number 82260379) and Xinjiang Uygur Autonomous Region Graduate Innovation Program (grant number XJ2024G157, XJ2024G147). No benefits in any form have been received or will be received from a commercial party related directly or indirectly to the subject of this article.

Disclosure

The authors report no conflicts of interest in this work.

References

1. Braun D. A retrospective review of the sepsis definition after publication of sepsis-3. *Am J Med*. 2019;132(3):382–384. doi:10.1016/j.amjmed.2018.11.003
2. Singer M, Deutschman CS, Seymour CW, et al. The third international consensus definitions for sepsis and septic shock (Sepsis-3). *JAMA*. 2016;315(8):801–810. doi:10.1001/jama.2016.0287
3. Klein Klouwenberg PM, Frencken JF, Kuipers S, et al. Incidence, predictors, and outcomes of new-onset atrial fibrillation in critically ill patients with sepsis. a cohort study. *Am J Respir Crit Care Med*. 2017;195(2):205–211. doi:10.1164/rccm.201603-0618OC
4. Xiao FP, Chen MY, Wang L, et al. Outcomes of new-onset atrial fibrillation in patients with sepsis: a systematic review and meta-analysis of 225,841 patients. *Am J Emerg Med*. 2021;42:23–30. doi:10.1016/j.ajem.2020.12.062
5. Jentzer JC, Lawler PR, Van Houten HK, et al. Cardiovascular events among survivors of sepsis hospitalization: a retrospective cohort analysis. *J Am Heart Assoc*. 2023;12(3):e027813. doi:10.1161/JAHA.122.027813
6. Lee-Iannotti JK, Capampangan DJ, Hoffman-Snyder C, et al. New-onset atrial fibrillation in severe sepsis and risk of stroke and death: a critically appraised topic. *Neurologist*. 2012;18(4):239–243. doi:10.1097/NRL.0b013e31825fa850
7. Walkey AJ, Wiener RS, Ghobrial JM, et al. Incident stroke and mortality associated with new-onset atrial fibrillation in patients hospitalized with severe sepsis. *JAMA*. 2011;306(20):2248–2254. doi:10.1001/jama.2011.1615
8. Hesselkilde EZ, Carstensen H, Flethøj M, et al. Longitudinal study of electrical, functional and structural remodelling in an equine model of atrial fibrillation. *BMC Cardiovasc Disord*. 2019;19(1):228. doi:10.1186/s12872-019-1210-4
9. Ohmori H, Sakamoto SI, Miyagi Y, et al. Shunt and pace: a novel experimental model of atrial fibrillation with a volume-loaded left atrium. *Gen Thorac Cardiovasc Surg*. 2023;71(5):272–279. doi:10.1007/s11748-022-01866-8
10. Kazui T, Henn MC, Watanabe Y, et al. The impact of 6 weeks of atrial fibrillation on left atrial and ventricular structure and function. *J Thorac Cardiovasc Surg*. 2015;150(6):1602–1608. doi:10.1016/j.jtcvs.2015.08.105
11. Rittirsch D, Huber-Lang MS, Flierl MA, et al. Immunodesign of experimental sepsis by cecal ligation and puncture. *Nat Protoc*. 2009;4(1):31–36. doi:10.1038/nprot.2008.214
12. Bapat A, Schloss MJ, Yamazoe M, et al. A mouse model of atrial fibrillation in sepsis. *Circulation*. 2023;147(13):1047–1049. doi:10.1161/CIRCULATIONAHA.122.060317
13. Sun Z, Zhou D, Xie X, et al. Cross-talk between macrophages and atrial myocytes in atrial fibrillation. *Basic Res Cardiol*. 2016;111(6):63. doi:10.1007/s00395-016-0584-z
14. Wu Q, Zhong P, Ning P, et al. Treadmill training mitigates bone deterioration via inhibiting NLRP3/Caspase1/IL-1β signaling in aged rats. *BMC Musculoskelet Disord*. 2022;23(1):1089. doi:10.1186/s12891-022-06055-5
15. Waltz P, Carchman E, Gomez H, et al. Sepsis results in an altered renal metabolic and osmolyte profile. *J Surg Res*. 2016;202(1):8–12. doi:10.1016/j.jss.2015.12.011
16. Wang N, Liu X, Zheng X, et al. Ulinastatin is a novel candidate drug for sepsis and secondary acute lung injury, evidence from an optimized CLP rat model. *Int Immunopharmacol*. 2013;17(3):799–807. doi:10.1016/j.intimp.2013.09.004
17. Ghavimi H, Sheidaei S, Vaez H, et al. Metformin-attenuated sepsis-induced oxidative damages: a novel role for metformin. *Iran J Basic Med Sci*. 2018;21(5):469–475. doi:10.22038/IJBMS.2018.24610.6126
18. Zhang B, Liu C, Yang N, et al. A comparative study of changes of autophagy in rat models of CLP versus LPS induced sepsis. *Exp Ther Med*. 2017;14(3):2194–2200. doi:10.3892/etm.2017.4758
19. Chancharoenthana W, Sutnu N, Visitchanakun P, et al. Critical roles of sepsis-reshaped fecal virota in attenuating sepsis severity. *Front Immunol*. 2022;13:940935. doi:10.3389/fimmu.2022.940935

20. McCarron EP, Williams DP, Antoine DJ, et al. Exploring the translational disconnect between the murine and human inflammatory response: analysis of LPS dose-response relationship in murine versus human cell lines and implications for translation into murine models of sepsis. *J Inflamm Res*. 2015;8:201–209. doi:10.2147/JIR.S89097
21. Seemann S, Zohles F, Lupp A. Comprehensive comparison of three different animal models for systemic inflammation. *J Biomed Sci*. 2017;24 (1):60. doi:10.1186/s12929-017-0370-8
22. Fang J, Kong B, Shuai W, et al. Ferroportin-mediated ferroptosis involved in new-onset atrial fibrillation with LPS-induced endotoxemia. *Eur J Pharmacol*. 2021;913:174622. doi:10.1016/j.ejphar.2021.174622
23. He D, Ruan ZB, Song GX, et al. miR-15a-5p regulates myocardial fibrosis in atrial fibrillation by targeting Smad7. *PeerJ*. 2021;9:e12686. doi:10.7717/peerj.12686
24. Jia Z, Wang J, Shi Q, et al. SOX6 and PDCD4 enhance cardiomyocyte apoptosis through LPS-induced miR-499 inhibition. *Apoptosis*. 2016;21 (2):174–183. doi:10.1007/s10495-015-1201-6
25. Aoki Y, Hatakeyama N, Yamamoto S, et al. Role of ion channels in sepsis-induced atrial tachyarrhythmias in Guinea pigs. *Br J Pharmacol*. 2012;166(1):390–400. doi:10.1111/j.1476-5381.2011.01769.x
26. Andrew CY, Klein AL. Role of echocardiography in atrial fibrillation ablation. *J Atr Fibrillation*. 2011;4(4):397. doi:10.4022/jafib.397
27. Ravelli F, Masè M, Del Greco M, et al. Acute atrial dilatation slows conduction and increases AF vulnerability in the human atrium. *J Cardiovasc Electrophysiol*. 2011;22(4):394–401. doi:10.1111/j.1540-8167.2010.01939.x
28. Dent JM. Role of echocardiography in the evaluation and management of atrial fibrillation. *Cardiol Clin*. 1996;14(4):543–553. doi:10.1016/s0733-8651(05)70303-9
29. Viola F, Bustamante M, Bolger A, et al. Diastolic function assessment with four-dimensional flow cardiovascular magnetic resonance using automatic deep learning E/A ratio analysis. *J Cardiovasc Magn Reson*. 2024;26(1):101042. doi:10.1016/j.jocmr.2024.101042
30. Ozdemir K, Altunkeser BB, Sökmen G, et al. Usefulness of peak mitral inflow velocity to predict severe mitral regurgitation in patients with normal or impaired left ventricular systolic function. *Am Heart J*. 2001;142(6):1065–1071. doi:10.1067/mhj.2001.118465
31. Mawatari K, Sanada JI. Tanaka Y, et al.Left ventricular systolic blood flow dynamics and left ventricular wall motion abnormalities in atrial fibrillation. *J Cardiol*. 1988;18(3):803–811.
32. Okuhara Y, Yokoe S, Iwasaku T, et al. Interleukin-18 gene deletion protects against sepsis-induced cardiac dysfunction by inhibiting PP2A activity. *Int J Cardiol*. 2017;243:396–403. doi:10.1016/j.ijcard.2017.04.082
33. Nemoto S, Vallejo JG, Knuefermann P, et al. Escherichia coli LPS-induced LV dysfunction: role of toll-like receptor-4 in the adult heart. *Am J Physiol Heart Circ Physiol*. 2002;282(6):H2316–H2323. doi:10.1152/ajpheart.00763.2001
34. Lyngbakken MN, Rønningen PS, Solberg MG, et al. Prediction of incident atrial fibrillation with cardiac biomarkers and left atrial volumes. *Heart*. 2023;109(5):356–363. doi:10.1136/heartjnl-2022-321608
35. Pruvot E, Jousset F, Ruchat P, et al. Propagation velocity kinetics and repolarization alternans in a free-behaving sheep model of pacing-induced atrial fibrillation. *Europace*. 2007;9(Suppl 6):vi83–vi88. doi:10.1093/europace/eum211
36. Daoud EG, Bogun F, Goyal R, et al. Effect of atrial fibrillation on atrial refractoriness in humans. *Circulation*. 1996;94(7):1600–1606. doi:10.1161/01.cir.94.7.1600
37. Yao C, Veleva T, L S Jr, et al. Enhanced Cardiomyocyte NLRP3 inflammasome signaling promotes atrial fibrillation. *Circulation*. 2018;138 (20):2227–2242. doi:10.1161/CIRCULATIONAHA.118.035202
38. Hobai IA, Morse JC, Siwik DA, et al. Lipopolysaccharide and cytokines inhibit rat cardiomyocyte contractility in vitro. *J Surg Res*. 2015;193 (2):888–901. doi:10.1016/j.jss.2014.09.015
39. Rossignol B, Gueret G, Pennec JP, et al. Effects of chronic sepsis on the voltage-gated sodium channel in isolated rat muscle fibers. *Crit Care Med*. 2007;35(2):351–357. doi:10.1097/01.CCM.0000254335.88023.0E
40. Collin S, Sennoun N, Dron AG, et al. Vascular ATP-sensitive potassium channels are over-expressed and partially regulated by nitric oxide in experimental septic shock. *Intensive Care Med*. 2011;37(5):861–869. doi:10.1007/s00134-011-2169-5
41. Sahoo N, Hoshi T, Heinemann SH. Oxidative modulation of voltage-gated potassium channels. *Antioxid Redox Signal*. 2014;21(6):933–952. doi:10.1089/ars.2013.5614
42. Tök L, Nazıroğlu M, Uğuz AC, et al. Elevated hydrostatic pressures induce apoptosis and oxidative stress through mitochondrial membrane depolarization in PC12 neuronal cells: a cell culture model of glaucoma. *J Recept Signal Transduction Res*. 2014;34(5):410–416. doi:10.3109/10799893.2014.910812
43. Ishii Y, Schuessler RB, Gaynor SL, et al. Postoperative atrial fibrillation: the role of the inflammatory response. *J Thorac Cardiovasc Surg*. 2017;153(6):1357–1365. doi:10.1016/j.jtcvs.2016.12.051
44. Murakami T, Ockinger J, Yu J, et al. Critical role for calcium mobilization in activation of the NLRP3 inflammasome. *Proc Natl Acad Sci U S A*. 2012;109(28):11282–11287. doi:10.1073/pnas.1117765109
45. Shi X, Tan S, Tan S. NLRP3 inflammasome in sepsis (Review). *Mol Med Rep*. 2021;24(1):514. doi:10.3892/mmr.2021.12153
46. Chai R, Ye Z, Xue W, et al. Tanshinone IIA inhibits cardiomyocyte pyroptosis through TLR4/NF-κB p65 pathway after acute myocardial infarction. *Front Cell Dev Biol*. 2023;11:1252942. doi:10.3389/fcell.2023.1252942
47. Che J, Wang H, Dong J, et al. Human umbilical cord mesenchymal stem cell-derived exosomes attenuate neuroinflammation and oxidative stress through the NRF2/NF-κB/NLRP3 pathway. *CNS Neurosci Ther*. 2024;30(3):e14454. doi:10.1111/cns.14454
48. Vigneron C, Py BF, Monneret G, et al. The double sides of NLRP3 inflammasome activation in sepsis. *Clin Sci (Lond)*. 2023;137(5):333–351. doi:10.1042/CS20220556
49. Lee CH, Choi JW. S1P/S1P2 signaling axis regulates both NLRP3 Upregulation and NLRP3 Inflammasome activation in macrophages primed with lipopolysaccharide. *Antioxidants*. 2021;10(11):1706. doi:10.3390/antiox10111706
50. Hou L, Zhang Z, Yang L, et al. NLRP3 inflammasome priming and activation in cholestatic liver injury via the sphingosine 1-phosphate/S1P receptor 2/Gα(12/13)/MAPK signaling pathway. *J Mol Med*. 2021;99(2):273–288. doi:10.1007/s00109-020-02032-4
51. Zeng H, Zou P, Chen Y, et al. NOX4 aggravates doxorubicin-induced cardiomyocyte pyroptosis by increasing reactive oxygen species content and activating the NLRP3 inflammasome. *Cardiovasc Diagn Ther*. 2024;14(1):84–100. doi:10.21037/cdt-23-142
52. Fang L, Ellims AH, Beale AL, et al. Systemic inflammation is associated with myocardial fibrosis, diastolic dysfunction, and cardiac hypertrophy in patients with hypertrophic cardiomyopathy. *Am J Transl Res*. 2017;9(11):5063–5073.

53. Xu B, Bai B, Sha S, et al. Interleukin-1β induces autophagy by affecting calcium homeostasis and trypsinogen activation in pancreatic acinar cells. *Int J Clin Exp Pathol*. 2014;7(7):3620–3631.
54. Xu Z, Zhang L, Pan Q, et al. Expression and Potential Significance of miR-499 and IL-1β in Serum of Dilated Cardiomyopathy Patients with Atrial Fibrillation. *Altern Ther Health Med*. 2024;29:AT10181
55. Cui L, Li C, Zhang G, et al. S1P/S1PR2 promote pancreatic stellate cell activation and pancreatic fibrosis in chronic pancreatitis by regulating autophagy and the NLRP3 inflammasome. *Chem Biol Interact*. 2023;380:110541. doi:10.1016/j.cbi.2023.110541
56. Sapkota A, Gaire BP, Kang MG, Choi JW. S1P2 contributes to microglial activation and M1 polarization following cerebral ischemia through ERK1/2 and JNK. *Sci Rep*. 2019;9(1):12106. doi:10.1038/s41598-019-48609-z
57. Shi Y, Zhao L, Wang J, et al. The selective NLRP3 inflammasome inhibitor MCC950 improves isoproterenol-induced cardiac dysfunction by inhibiting cardiomyocyte senescence. *Eur J Pharmacol*. 2022;937:175364. doi:10.1016/j.ejphar.2022.175364